Kwangjin Lee

J. R. Barber

Department of Mechanical Engineering
and Applied Mechanics,
University of Michigan,
Ann Arbor, MI 48109-2125

Frictionally Excited Thermoelastic Instability in Automotive Disk Brakes

Thermoelastic instability in automotive disk brake systems is investigated focusing on the effect of a finite disk thickness. A finite layer model with an antisymmetric mode of deformation can estimate the onset of instability observed in actual disk brake systems. Also some effects of system parameters on stability are found to agree well to experimental observations.

1 Introduction

Dow and Burton (1972) and Burton et al. (1973) have shown that a small sinusoidal perturbation in the otherwise uniform contact pressure between two sliding half-planes is unstable if the sliding speed exceeds a certain critical value which depends upon the wavelength of the perturbation. This instability, which results from the interaction of frictional heat generation, thermoelastic distortion and elastic contact, is known as frictionally excited thermoelastic instability or TEI (Barber, 1967 and 1969). It leads generally to the establishment of localized high temperature contact regions known as *hot spots*. This phenomenon is observed in many practical applications, particularly in brakes and clutches, where significant frictional heating occurs (Swaaij, 1979; Hewitt and Musial, 1979; Kreitlow et al., 1985; Abendroth, 1985; Anderson and Knapp, 1989). Severe hot spotting may produce harmful surface cracks (Anderson and Knapp, 1989) and induce low frequency vibration problems (Kreitlow et al., 1985; Thomas, 1988).

Burton's analysis can be used to obtain an order of magnitude estimate of the speed required to cause TEI, but this estimate is found to be considerably higher than the speeds at which hot spots are observed experimentally in automotive disk brake systems (Kreitlow et al., 1985; Abendroth, 1985; Anderson and Knapp, 1989). An important factor in this discrepancy is probably associated with the difference in geometry in that the brake disk has a finite thickness and slides against two pads, one on each side, in contrast to Burton's system of two sliding half-planes with a single interface. In particular, we might anticipate that the finite disk dimension will exert a stabilizing influence on the longer wavelength perturbations, which are those governing the onset of instability.

In the present paper, we shall examine this hypothesis by extending Burton's analysis to the case of a layer sliding between two half-planes.

2 The Model

We represent the brake disk by a layer of thickness $2a$ and the pads by two half-planes, as shown in Fig. 1. The stationary half-planes, 1, are pressed together by a uniform pressure p_0 and the disk, 2, slides between them at constant speed V.

It might be argued that the representation of finite thickness pads by half-planes in this model will introduce errors comparable with the effects under investigation, but this will not be the case as long as the conductivity of the pad material is significantly lower than that for the disk. Burton has shown that in such circumstances, the pressure perturbation is almost stationary with respect to the good conductor and moves over the surface of the poor conductor. The perturbed temperature field then penetrates only a small distance below the surface of the poor conductor and hence replacement of a finite thickness pad by a half-plane will have little effect on the resulting stability behavior.

In automotive practice, disks are typically of cast iron (K = 54 W/m°C) and composition friction materials are used for the pad with conductivities generally lower than 57 W/m°C.

The geometry of the system is symmetrical about the midplane of the layer, but it does not necessarily follow that an unstable perturbation will exhibit the same symmetry. How-

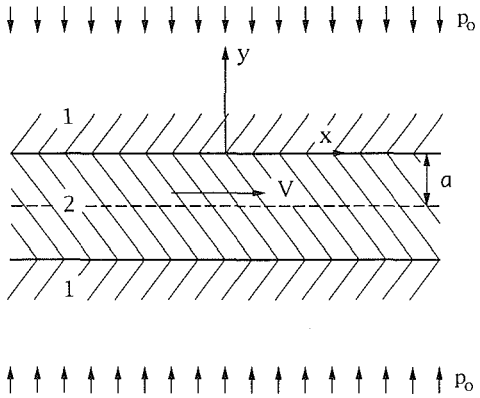

Fig. 1 A layer between two half-planes, pressed by a uniform pressure p_0

Contributed by the Tribology Division for publication in the JOURNAL OF TRIBOLOGY. Manuscript received by the Tribology Division July 7, 1992; revised manuscript received October 1992. Associate Technical Editor: M. Godet.

ever, as long as the perturbation remains small, linearity is preserved and it follows that we can describe an arbitrary disturbance as the sum of symmetric and anti-symmetric parts. Furthermore, unless two or more unstable perturbations have the same exponential growth rate, the stability boundary and the growth of the resulting disturbance will be dominated by the leading symmetric or anti-symmetric mode. We therefore consider the symmetric and antisymmetric problems separately and discuss the consequences for the more general problem in section 5.

3 The Symmetric Problem

Following Dow and Burton (1972) and Burton et al. (1973), we examine the conditions under which a spatially sinusoidal perturbation in the stress and temperature fields can grow exponentially with time, t. Results for a more general form of perturbation can then be obtained by superposition, which in this instance would be equivalent to Fourier transformation.

The half-planes and the layer are generally of dissimilar materials, appropriate properties being distinguished by the suffix 1 for the half-planes and 2 for the layer. We assume that the perturbation has an absolute velocity c in the x-direction and relative velocity c_i with respect to body i. It follows that $c = c_1 = V + c_2$ and that the sliding velocity V can be written

$$V = c_1 - c_2 \tag{1}$$

We introduce the coordinate system (x, y) moving with the perturbed field, so that the perturbation in contact pressure can be written as

$$p(x,t) = p_1 \exp(bt)\cos(mx) \tag{2}$$

The associated perturbation in frictional heat generated is then given by

$$q_{\text{net}} = q_{y1} - q_{y2} = fVp_1 \exp(bt)\cos(mx) \tag{3}$$

where f is the coefficient of friction and q_{yi} is the heat flux in the y-direction at the interface in body i.

We also introduce local coordinate systems (x_i, y_i), stationary in the upper half-plane and the disk respectively, through the relations

$$x = x_1 - c_1 t \tag{4}$$

$$= x_2 - c_2 t \tag{5}$$

$$y = y_1 \tag{6}$$

$$= y_2 - a \tag{7}$$

3.1 Temperature Field. The temperature field in each body must satisfy the transient heat conduction equation

$$\frac{\partial^2 T_i}{\partial x_i^2} + \frac{\partial^2 T_i}{\partial y_i^2} = \frac{1}{k_i}\frac{\partial T_i}{\partial t} \tag{8}$$

where

$$k_i = \frac{K_i}{\rho_i c_{pi}} \tag{9}$$

is the thermal diffusivity and K_i, ρ_i, c_{pi} are, respectively, the thermal conductivity, density, and specific heat of the material.

A suitable form of temperature perturbation can be written in the form

$$T_i = \Re\{f_i(y_i)\exp(bt + jm(x_i - c_i t))\} \tag{10}$$

where $j = \sqrt{-1}$ and the (generally complex) function $f_i(y_i)$ has to be chosen to satisfy (8). Note that in the following analysis we shall assume that the exponential growth rate b is real. Substituting (10) into (8) and solving the resulting ordinary differential equation, we obtain

$$f_i(y_i) = F_i \exp(-\lambda_i y_i) + G_i \exp(\lambda_i y_i) \tag{11}$$

where

$$\lambda_i \equiv \xi_i + j\eta_i = \sqrt{\left(m^2 + \frac{b}{k_i}\right) - \frac{jmc_i}{k_i}}, \tag{12}$$

F_i, G_i are arbitrary complex constants and the square root is defined such that $\xi_i > 0$. Thus we have

$$T_i = \Re\{(F_i \exp(-\lambda_i y_i) + G_i \exp(\lambda_i y_i))\exp(bt + jm(x_i - c_i t))\} \tag{13}$$

The temperature perturbation in body 1 must decay away from the interface, i.e., $T_1 \to 0$ as $y_1 \to \infty$, from which we conclude that $G_1 = 0$ and hence

$$T_1 = \Re\{F_1 \exp(bt - \lambda_1 y_1 + jm(x_1 - c_1 t))\} \tag{14}$$

Also, from the symmetry of the problem, we have

$$q_{y2} = -K_2 \left.\frac{\partial T_2}{\partial y_2}\right|_{y_2 = 0} = 0 \tag{15}$$

Nomenclature

- A = dimensionless half layer thickness
- a = half layer thickness
- b = exponential growth rate
- b^* = dimensionless exponential growth rate
- c = absolute velocity of perturbation
- c_i = relative velocity of perturbation with respect to body i
- c_i^* = dimensionless relative velocity of perturbation with respect to body i
- c_p = specific heat
- E = elastic modulus
- f = coefficient of friction
- j = $\sqrt{-1}$
- K = thermal conductivity
- K^* = ratio of thermal conductivities
- k = thermal diffusivity
- k^* = ratio of thermal diffusivities
- l = wavelength
- l_p = pad length
- m = spatial frequency of sinusoidal perturbation
- p = pressure perturbation
- q_{net} = perturbation in frictional heat
- q_y = heat flux in the y-direction
- $\Re$ = real part of complex function
- T = temperature perturbation
- t = time
- u = displacement
- V = sliding velocity
- V^* = dimensionless sliding velocity
- x = coordinate in sliding direction moving with the perturbed field
- x_i = local coordinate in x-direction stationary in body i
- y = coordinate in direction of disk thickness moving with the perturbed field
- y_i = local coordinate in y-direction stationary in body i
- α = coefficient of thermal expansion
- α^* = dimensionless coefficient of thermal expansion
- η = imaginary part of λ
- λ = separation constant
- λ^* = dimensionless λ
- μ = shear modulus
- ν = Poisson's ratio
- ξ = real part of λ
- ρ = density
- σ = stress
- ϕ = isothermal potential A
- ψ = thermoelastic potential
- ω = isothermal potential D

Subscripts

- 1 = half-planes
- 2 = layer

which with (13) implies

$$F_2 = G_2 \tag{16}$$

Thus, the temperature in body 2 can be written

$$T_2 = \Re\{2F_2 \cosh(\lambda_2 y_2)\exp(bt + jm(x_2 - c_2 t))\} \tag{17}$$

The temperature is required to be continuous at the interface, i.e.,

$$T_1(x,0,t) = T_2(x,0,t) \tag{18}$$

Expressing (14) and (17) in the (x, y) coordinate system and using (18), we obtain

$$F_1 = 2F_2 \cosh(\lambda_2 a) \tag{19}$$

Thus, we can write the temperature in the (x, y) coordinate system in the form

$$T_1 = \Re\{T_0 \exp(bt - \lambda_1 y + jmx)\} \tag{20}$$

$$T_2 = \Re\left\{T_0 \frac{\cosh(\lambda_2(y+a))}{\cosh(\lambda_2 a)} \exp(bt + jmx)\right\} \tag{21}$$

where T_0 is an unknown constant. Note that only the heat conduction equation contains time-dependent terms and hence the subsequent calculations can all be performed in the moving coordinate system (x, y).

3.2 The Heat Generated at the Interface. The heat flux at the interface[1] can be written

$$q_{yi} = -K_i \frac{\partial T_i}{\partial y}\bigg|_{y=0} \tag{22}$$

Substituting (20) and (21) into (22) and using (3), we obtain

$$fVp_1 \exp(bt)\cos(mx) = \Re\{\{K_1\lambda_1 + K_2\lambda_2 \tanh(\lambda_2 a)\} T_0 \exp(bt + jmx)\} \tag{23}$$

and hence

$$\{K_1\lambda_1 + K_2\lambda_2 \tanh(\lambda_2 a)\} T_0 = fVp_1 \tag{24}$$

3.3 Thermoelastic Stresses and Displacements. We now consider the mechanical boundary conditions of the problem. Since the stresses due to the temperature perturbation must disappear at a distance far from the interface, we have a boundary condition at infinity such that

$$\sigma_{xx1},\ \sigma_{xy1},\ \sigma_{yy1} \to 0 \quad y \to \infty \tag{25}$$

Also, from the symmetry of the problem, we have

$$u_{y2} = 0 \quad y = -a \tag{26}$$

$$\sigma_{xy2} = 0 \quad y = -a \tag{27}$$

At the interface, $y = 0$, we have

$$u_{y1} = u_{y2} \tag{28}$$

$$\sigma_{yy1} = \sigma_{yy2} = -p(x,t) \tag{29}$$

$$\sigma_{xy1} = \sigma_{xy2} = -fp(x,t) \tag{30}$$

where the sign in Eq. (30) implies that $V > 0$.

A particular solution of the thermoelastic problem corresponding to the temperature field of (20) and (21) can be obtained in terms of a strain function ψ (see Barber, 1992, Chapter 17).

$$2\mu \underline{u_i} = \underline{\nabla}\psi_i \tag{31}$$

where

$$\nabla^2 \psi_i = \beta_i T_i \tag{32}$$

$$\beta_i \equiv \frac{2\mu_i \alpha_i (1+\nu_i)}{1-\nu_i} \tag{33}$$

and α_i, μ_i, ν_i are, respectively, the coefficient of thermal expansion, shear modulus, and Poisson's ratio of the materials. Substituting (20) and (21) into (32) we obtain

$$\psi_1 = \Re\left\{\frac{\beta_1 T_0}{\lambda_1^2 - m^2} \exp(bt - \lambda_1 y + jmx)\right\} \tag{34}$$

$$\psi_2 = \Re\left\{\frac{\beta_2 T_0}{\lambda_2^2 - m^2} \frac{\cosh(\lambda_2(y+a))}{\cosh(\lambda_2 a)} \exp(bt + jmx)\right\} \tag{35}$$

The corresponding stresses and normal displacements are defined through the relations

$$u_{yi} = \frac{1}{2\mu_i}\frac{\partial \psi_i}{\partial y};\quad \sigma_{yyi} = -\frac{\partial^2 \psi_i}{\partial x^2};\quad \sigma_{xyi} = \frac{\partial^2 \psi_i}{\partial x \partial y} \tag{36}$$

We next superpose isothermal solutions A and D of Green and Zerna (1954, section 5.7) on the particular solution (36) to obtain a sufficiently general solution to satisfy the mechanical boundary conditions. The corresponding stress and displacement components are

$$u_{y1} = \frac{1}{2\mu_1}\frac{\partial \phi_1}{\partial y} + \frac{1}{2\mu_1}\left\{y\frac{\partial \omega_1}{\partial y} - (3 - 4\nu_1)\omega_1\right\} \tag{37}$$

$$\sigma_{yy1} = -\frac{\partial^2 \phi_1}{\partial x^2} + y\frac{\partial^2 \omega_1}{\partial y^2} - 2(1-\nu_1)\frac{\partial \omega_1}{\partial y} \tag{38}$$

$$\sigma_{xy1} = \frac{\partial^2 \phi_1}{\partial x \partial y} + y\frac{\partial^2 \omega_1}{\partial x \partial y} - (1 - 2\nu_1)\frac{\partial \omega_1}{\partial x} \tag{39}$$

$$u_{y2} = \frac{1}{2\mu_2}\frac{\partial \phi_2}{\partial y} + \frac{1}{2\mu_2}\left\{(y+a)\frac{\partial \omega_2}{\partial y} - (3 - 4\nu_2)\omega_2\right\} \tag{40}$$

$$\sigma_{yy2} = -\frac{\partial^2 \phi_2}{\partial x^2} + (y+a)\frac{\partial^2 \omega_2}{\partial y^2} - 2(1-\nu_2)\frac{\partial \omega_2}{\partial y} \tag{41}$$

$$\sigma_{xy2} = \frac{\partial^2 \phi_2}{\partial x \partial y} + (y+a)\frac{\partial^2 \omega_2}{\partial x \partial y} - (1 - 2\nu_2)\frac{\partial \omega_2}{\partial x} \tag{42}$$

where $\nabla^2 \phi_i,\ \omega_i = 0$. Notice that, for the layer, we have chosen to preserve the symmetry of the representation by writing the solution initially in the (x_2, y_2) coordinate system and then using the relation $y_2 = y + a$. This change of coordinate system only affects the terms deriving from solution D—i.e., those involving ω_2. We can then satisfy the symmetry conditions (26, 27) by requiring that ϕ_2 be an even function and ω_2 an odd function of $y_2 = (y + a)$, the appropriate forms being

$$\phi_2 = \Re\{A_2 \cosh(m(y+a))\exp(jmx)\} \tag{43}$$

$$\omega_2 = \Re\{B_2 \sinh(m(y+a))\exp(jmx)\} \tag{44}$$

To satisfy (25) we choose ϕ_1, ω_1 such that $\phi_1,\ \omega_1 \to 0$ as $y \to \infty$. Suitable forms are

$$\phi_1 = \Re\{A_1 \exp(-my + jmx)\} \tag{45}$$

$$\omega_1 = \Re\{B_1 \exp(-my + jmx)\} \tag{46}$$

Substituting (34–35) into (36) and (43–46) into (37–42) respectively and superposing corresponding stress and displacement components, we obtain

$$u_{y1} = \Re\left[-\frac{1}{2\mu_1}\left\{\frac{\beta_1 T_0 \lambda_1}{\lambda_1^2 - m^2}\exp(-\lambda_1 y + bt + jmx)\right\} - \frac{1}{2\mu_1}\{mA_1 \exp(-my + jmx)\} - \frac{1}{2\mu_1}\{my + (3 - 4\nu_1)\}B_1 \exp(-my + jmx)\right] \tag{47}$$

[1]Notice that there is also heat generated at the symmetric interface $y = -2a$, but this is automatically accounted for by the symmetry condition (15).

$$H_1(A)=\frac{2\mu_1\mu_2k_2\alpha_2(1+\nu_2)}{\{\mu_2(1-\nu_1)(A\text{sech}^2A+\tanh A)+\mu_1(1-\nu_2)\tanh^2A\}K_2}, \quad (55)$$

$$H_2(A)=\frac{4\mu_1\mu_2k_2\alpha_2(1+\nu_2)}{\{\mu_2(1-2\nu_1)(A\text{sech}^2A+\tanh A)-\mu_1(1-2\nu_2)\tanh A+\mu_1A\text{sech}^2A\}K_2} \quad (56)$$

$$\sigma_{yy1}=\Re\left[m^2\left\{\frac{\beta_1T_0}{\lambda_1^2-m^2}\exp(-\lambda_1y+bt+jmx)\right\}+m^2A_1\exp(-my+jmx)+\{my+2(1-\nu_1)\}mB_1\exp(-my+jmx)\right] \quad (48)$$

$$\sigma_{xy1}=\Re\left[-jm\left\{\frac{\beta_1T_0\lambda_1}{\lambda_1^2-m^2}\exp(-\lambda_1y+bt+jmx)\right\}-jm^2A_1\exp(-my+jmx)-j\{my+(1-2\nu_1)\}mB_1\exp(-my+jmx)\right] \quad (49)$$

$$u_{y2}=\Re\left[\frac{1}{2\mu_2}\left\{\frac{\beta_2T_0\lambda_2}{\lambda_2^2-m^2}\frac{\sinh(\lambda_2(y+a))}{\cosh(\lambda_2a)}\exp(bt+jmx)\right\}+\frac{1}{2\mu_2}\{mA_2\sinh(m(y+a))\exp(jmx)\}+\frac{1}{2\mu_2}\{(y+a)m\cosh(m(y+a))-(3-4\nu_2)\sinh(m(y+a))\}\times B_2\exp(jmx)\right] \quad (50)$$

$$\sigma_{yy2}=\Re\left[m^2\left\{\frac{\beta_2T_0}{\lambda_2^2-m^2}\frac{\cosh(\lambda_2(y+a))}{\cosh(\lambda_2a)}\exp(bt+jmx)\right\}+m^2A_2\cosh(m(y+a))\exp(jmx)+\{(y+a)m\sinh(m(y+a))-2(1-\nu_2)\cosh(m(y+a))\}\times mB_2\exp(jmx)\right] \quad (51)$$

$$\sigma_{xy2}=\Re\left[jm\left\{\frac{\beta_2T_0\lambda_2}{\lambda_2^2-m^2}\frac{\sinh(\lambda_2(y+a))}{\cosh(\lambda_2a)}\exp(bt+jmx)\right\}+jm^2A_2\sinh(m(y+a))\exp(jmx)+j\{(y+a)m\cosh(m(y+a))-(1-2\nu_2)\sinh(m(y+a))\}\times mB_2\exp(jmx)\right] \quad (52)$$

The interface conditions (28–30) then define four simultaneous complex equations for the complex constants, A_1, A_2, B_1, B_2. Finally, noting that the contact traction

$$\sigma_{yy1}(x,0,t)=-p_1\exp(bt)\cos(mx), \quad (53)$$

we can substitute for p_1 in Eq. (24) to obtain the complex characteristic equation

$$\left\{\frac{K_1}{K_2}\lambda_1+\lambda_2\tanh(\lambda_2a)\right\}\left(1-jf\frac{H_1}{H_2}\right)=\frac{fH_1Vm}{k_2}\left[\frac{1}{\lambda_1+m}\frac{\alpha_1(1+\nu_1)}{\alpha_2(1+\nu_2)}\{A\text{sech}^2A+\tanh A\}+\frac{\tanh A}{\lambda_2^2-m^2}\{\lambda_2\tanh(\lambda_2a)-m\tanh A\}\right] \quad (54)$$

where

and $A = ma$.

For given values of V, m and material properties, Eq. (54) defines the exponential growth rate b, which appears implicitly in λ_i through Eq. (12).

3.4 Dimensionless Presentation. We restate the characteristic Eq. (54) in dimensionless form by defining the following dimensionless parameters.

$$K^*=\frac{K_1}{K_2};\quad k^*=\frac{k_1}{k_2};\quad \alpha^*=\frac{\alpha_1(1+\nu_1)}{\alpha_2(1+\nu_2)} \quad (57)$$

$$\lambda_i^*=\frac{\lambda_1}{m};\quad c_i^*=\frac{c_i}{k_2m} \quad (58)$$

$$V^*=\frac{V}{k_2m}=c_1^*-c_2^* \quad (59)$$

$$b^*=\frac{b}{k_2m^2} \quad (60)$$

Substituting the expressions (57–59) into Eq. (54), we have

$$\{K^*\lambda_1^*+\lambda_2^*\tanh(\lambda_2^*A)\}\left(1-jf\frac{H_1}{H_2}\right)=fH_1V^*\left[\frac{\alpha^*}{\lambda_1^*+1}(A\text{sech}^2A+\tanh A)+\frac{\tanh A}{\lambda_2^{*2}-1}\times\{\lambda_2^*\tanh(\lambda_2^*A)-\tanh A\}\right] \quad (61)$$

3.5 The Stability Boundary. Perturbations will generally only be possible for certain eigenvalues of the exponential growth rate, b. Stability will be maintained if the growth rates of all such perturbations are negative since all initial perturbations will then decay with time. Thus we can find the stability boundary by setting the growth rate to zero and hence obtain the critical sliding speed which depends upon the wavelength of the perturbation. When $b = 0$, the dimensionless form of Eq. (12) reduces to

$$\lambda_i^*\equiv\xi_i^*+j\eta_i^* \quad (62)$$

where

$$\xi_1^*=\left\{\frac{1}{2}\left[1+\sqrt{1+\left(\frac{c_1^*}{k^*}\right)^2}\right]\right\}^{1/2} \quad (63)$$

$$\eta_1^*=-\left\{\frac{1}{2}\left[-1+\sqrt{1+\left(\frac{c_1^*}{k^*}\right)^2}\right]\right\}^{1/2} \quad (64)$$

$$\xi_2^*=\left\{\frac{1}{2}\left[1+\sqrt{1+(c_2^*)^2}\right]\right\}^{1/2} \quad (65)$$

$$\eta_2^*=\left\{\frac{1}{2}\left[-1+\sqrt{1+(c_2^*)^2}\right]\right\}^{1/2} \quad (66)$$

which imply the relations

$$\xi_1^{*2}-\eta_1^{*2}=1;\quad \xi_2^{*2}-\eta_2^{*2}=1 \quad (67)$$

After substituting (62) into Eq. (61) and separating the real and imaginary parts, we obtain two real equations, which, using (67) can be written

$$K^*\xi_1^* + \frac{\xi_2^* \sinh(2A\xi_2^*) - \eta_2^* \sin(2A\eta_2^*)}{\cosh(2A\xi_2^*) + \cos(2A\eta_2^*)} + f\frac{H_1}{H_2}\left\{K^*\eta_1^* + \frac{\xi_2^* \sin(2A\eta_2^*) + \eta_2^* \sinh(2A\xi_2^*)}{\cosh(2A\xi_2^*) + \cos(2A\eta_2^*)}\right\} = \frac{fH_1V^*}{2}\left[\frac{\alpha^*}{\xi_1^*}(A\,\mathrm{sech}^2 A + \tanh A) + \frac{\tanh A}{\xi_2^*\eta_2^*} \times \left\{\frac{\xi_2^* \sin(2A\eta_2^*) + \eta_2^* \sinh(2A\xi_2^*)}{\cosh(2A\xi_2^*) + \cos(2A\eta_2^*)}\right\}\right] \quad (68)$$

$$K^*\xi_1^* + \frac{\xi_2^* \sinh(2A\xi_2^*) + \eta_2^* \sin(2A\eta_2^*)}{\cosh(2A\xi_2^*) - \cos(2A\eta_2^*)} + f\frac{H_1}{H_2}\left\{K^*\eta_1^* + \frac{\eta_2^* \sinh(2A\xi_2^*) - \xi_2^* \sin(2A\eta_2^*)}{\cosh(2A\xi_2^*) - \cos(2A\eta_2^*)}\right\} = \frac{fH_1V^*}{2}\left[\frac{\alpha^*}{\xi_1^*}(-A\,\mathrm{csch}^2 A + \coth A) + \frac{\coth A}{\xi_2^*\eta_2^*} \times \left\{\frac{\eta_2^* \sinh(2A\xi_2^*) - \xi_2^* \sin(2A\eta_2^*)}{\cosh(2A\xi_2^*) - \cos(2A\eta_2^*)}\right\}\right] \quad (76)$$

$$K^*\eta_1^* + \frac{\xi_2^* \sin(2A\eta_2^*) + \eta_2^* \sinh(2A\xi_2^*)}{\cosh(2A\xi_2^*) + \cos(2A\eta_2^*)} - f\frac{H_1}{H_2}\left\{K^*\xi_1^* + \frac{\xi_2^* \sinh(2A\xi_2^*) - \eta_2^* \sin(2A\eta_2^*)}{\cosh(2A\xi_2^*) + \cos(2A\eta_2^*)}\right\} = -\frac{fH_1V^*}{2}\left[\frac{\alpha^*\eta_1^*}{\xi_1^*(\xi_1^*+1)}(A\,\mathrm{sech}^2 A + \tanh A) + \frac{\tanh A}{\xi_2^*\eta_2^*}\left\{\frac{\xi_2^* \sinh(2A\xi_2^*) - \eta_2^* \sin(2A\eta_2^*) - \tanh A(\cosh(2A\xi_2^*) + \cos(2A\eta_2^*))}{\cosh(2A\xi_2^*) + \cos(2A\eta_2^*)}\right\}\right] \quad (69)$$

$$K^*\eta_1^* + \frac{-\xi_2^* \sin(2A\eta_2^*) + \eta_2^* \sinh(2A\xi_2^*)}{\cosh(2A\xi_2^*) - \cos(2A\eta_2^*)} - f\frac{H_1}{H_2}\left\{K^*\xi_1^* + \frac{\xi_2^* \sinh(2A\xi_2^*) + \eta_2^* \sin(2A\eta_2^*)}{\cosh(2A\xi_2^*) - \cos(2A\eta_2^*)}\right\} = -\frac{fH_1V^*}{2}\left[\frac{\alpha^*\eta_1^*}{\xi_1^*(\xi_1^*+1)} \times (-A\,\mathrm{csch}^2 A + \coth A) + \frac{\coth A}{\xi_2^*\eta_2^*}\left\{\frac{\xi_2^* \sinh(2A\xi_2^*) + \eta_2^* \sin(2A\eta_2^*) - \coth A(\cosh(2A\xi_2^*) - \cos(2A\eta_2^*))}{\cosh(2A\xi_2^*) - \cos(2A\eta_2^*)}\right\}\right] \quad (77)$$

These equations and the relation (59) can be used to eliminate c_1^*, c_2^* and hence determine the dimensionless critical speed V^*.

4 The Antisymmetric Problem

From the antisymmetry of the problem, we have

$$T_2 = 0 \quad y = -a \quad (70)$$

$$u_{x2} = 0 \quad y = -a \quad (71)$$

$$\sigma_{yy2} = 0 \quad y = -a \quad (72)$$

Following the same steps as the symmetric problem except using (70–72) instead of (15) and (26–27), we obtain the complex characteristic equation for antisymmetric problem, which, using (57–59) can be written

$$\{K^*\lambda_1^* + \lambda_2^* \coth(\lambda_2^* A)\}\left(1 - jf\frac{H_1}{H_2}\right) = fH_1V^*\left[\frac{\alpha^*}{\lambda_1^*+1}(-A\,\mathrm{csch}^2 A + \coth A) + \frac{\coth A}{\lambda_2^{*2}-1}\{\lambda_2^* \coth(\lambda_2^* A) - \coth A\}\right] \quad (73)$$

where

$$H_1(A) = \frac{2\mu_1\mu_2 k_2\alpha_2(1+\nu_2)}{\{\mu_2(1-\nu_1)(-A\,\mathrm{csch}^2 A + \coth A) + \mu_1(1-\nu_2)\coth^2 A\}K_2} \quad (74)$$

and

$$H_2(A) = \frac{4\mu_1\mu_2 k_2\alpha_2(1+\nu_2)}{\{\mu_2(1-2\nu_1)(-A\,\mathrm{csch}^2 A + \coth A) - \mu_1(1-2\nu_2)\coth A - \mu_1 A\,\mathrm{csch}^2 A\}K_2} \quad (75)$$

After substituting (62) into Eq. (73) and separating the real and imaginary parts, we obtain two real equations, which, using (67) can be written

As before, these equations and the relation (59) can be used to eliminate c_1^*, c_2^* and hence determine the dimensionless critical speed V^*.

5 Results

Grey cast iron is almost universally used for brake drums and disks, but there is considerably more variability in the choice of friction materials. Two typical friction materials—one asbestos-based (material C) and one semimetallic (material D)—are investigated in the present section, though we note that semimetallics have now largely replaced asbestos friction materials due to environmental concerns. Appropriate material properties, reproduced from Day (1988) are given in Table 1. Notice in particular that both friction materials have substantially lower thermal conductivity than cast iron, which is expected to cause the velocity of the self-excited perturbation to be closer to that of the disk than the pad. The difference in conductivities is not so large as to permit the simplifying ap-

Table 1 Material properties

No.	Material	E $N/m^2 \times 10^9$	ν	α $°C^{-1} \times 10^{-6}$	K W/m °C	k $m^2/s \times 10^{-6}$
1	Pad material C	.53	0.25	30	.5	.269
1	Pad material D	1	0.25	10	5.0	3.57
2	Cast iron	125	0.25	12	54	12.98

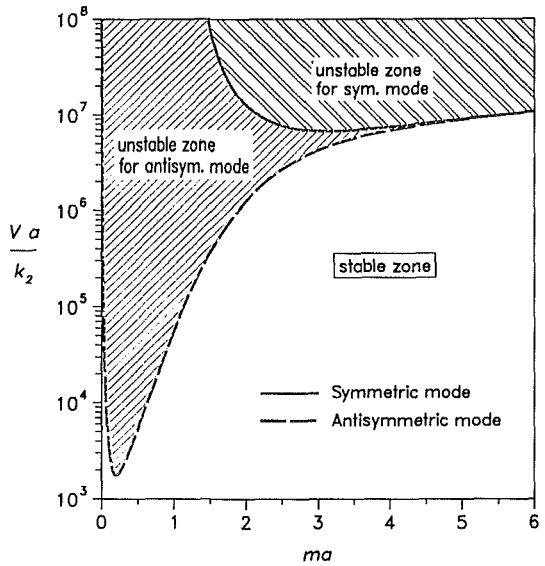

Fig. 2 The critical speed of the symmetric and antisymmetric modes of deformation for material C

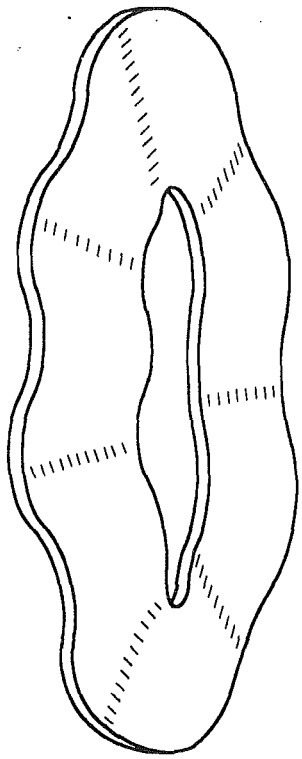

Fig. 3 Circumferentially buckled configuration for the disk

proximation of the pad material by a thermal insulator (Lee and Barber, 1993), but it will restrict the flow of heat into the pad and therefore justifies the representation of the pads by half-spaces instead of layers.

We take $f = 0.4$ as an appropriate value for the coefficient of friction (Day, 1988).

Symmetric and Antisymmetric Modes. The critical speed V—i.e., the sliding speed at which the perturbation first becomes unstable—is shown in Fig. 2 as a function of $A = ma$, for a sliding system of cast iron and friction material C. For a disk of given thickness, a, the dimensionless parameter A varies with the wavenumber m, or inversely with the wavelength l, since

$$A = ma = \frac{2\pi a}{l} \text{ and hence } l = \frac{2\pi a}{A} \tag{78}$$

Figure 2 shows that the antisymmetric mode becomes unstable at a lower speed than the symmetric mode for all values of the wavelength and hence practical instabilities are likely to be characterized by antisymmetric deformations. This is indeed confirmed by experiment and by service experience (Thoms, 1988). The antisymmetric mode involves hot spots located alternately on the two sides of the disk in the direction of sliding and leads to a circumferentially 'buckled' deformation pattern as shown in Fig. 3.

Qualitatively similar results were obtained with friction material D and also for hypothetical friction materials with a wide range of thermal properties.

5.1 The Effect of Wavelength. If the pad material and the disk were really semi-infinite in the direction of sliding, perturbations of any wavelength would be possible and the system would be unstable if any such perturbation were unstable in either the symmetric or antisymmetric mode. If the sliding speed were gradually increased from zero, instability would therefore first occur at the speed corresponding to the minimum in the antisymmetric curve in Fig. 2. This region of the curve is shown on an expanded scale in Fig. 4, which also shows the corresponding curve for the semimetallic friction material, D. In both cases, the minimum occurs at about $A = 0.2$, indicating that the initial instability will have a wavelength of $l \approx 30a$, from Eq. (78). Notice that l is also the anticipated spacing between hot spots on one side of the disk in the unstable configuration.

However, real brake systems have finite dimensions and these place restrictions on the permissible wavelength of perturbations. In particular, a brake pad of finite length must make contact at any given time with a sufficient number of hot spots to maintain kinematic support. Of course, the finite length of the pad strictly invalidates the present analysis, but we might reasonably suppose that the predicted unstable state will be a good approximation to the actual system if the pad is long enough to contain at least one full sinusoid of the perturbation[2]. This in turn restricts A in Fig. 4 to the range

$$\frac{2\pi a}{l_P} < A < \infty \tag{79}$$

where l_P is the pad length.

For typical dimensions used in automotive practice, this restriction is likely to an active constraint on A and hence on

[2]More precisely, a full perturbation analysis for the pad of finite length would generate a set of eigenvalues (critical speeds) and corresponding eigenfunctions (pressure perturbations) of approximately sinusoidal shape. Since the pressure perturbation must be self-equilibrating, the first appropriate sinusoidal form involves one complete wavelength.

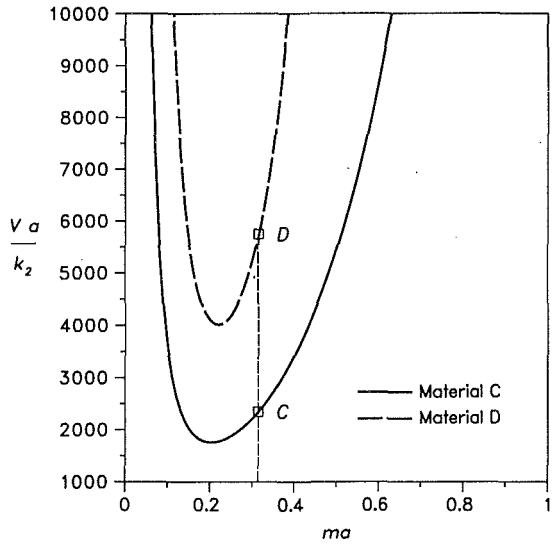

Fig. 4 The effect of wavelength on the critical speed near the minimum point

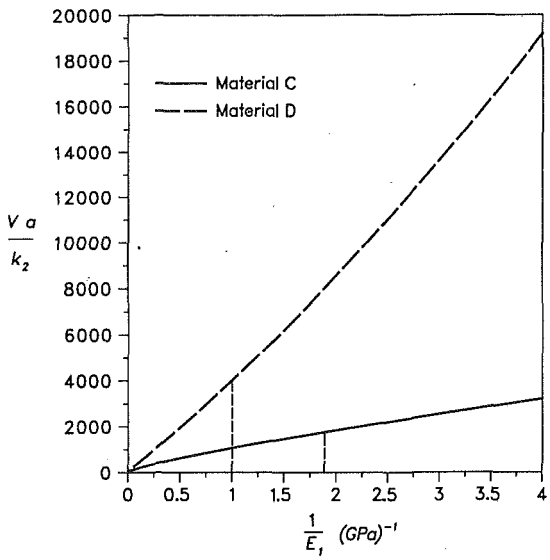

Fig. 5 The effect of elastic modulus on the minimum critical speed

the critical speed. For example, if the disk thickness is 10 mm (i.e., the half-thickness $a = 5$ mm), the preferred wavelength is about 150 mm and the corresponding dimensionless critical speed is 1759 for friction material C and 4010 for material D. These values are equivalent to sliding speeds of 4.6 m/s for material C and 10.4 m/s for material D, in dimensional terms. However, if the actual pad length is only 100 mm, such a long wavelength perturbation cannot be supported. If we assume that the longest permissible wavelength is equal to the pad length—i.e., $l = 100$ mm and $A = 0.314$—only the region to the right of the vertical line in Fig. 4 describes physically possible perturbations. The dimensionless critical speed then corresponds to the points C, D in Fig. 4, being increased to 2350 for material C and 5750 for material D. The corresponding dimensional values are 6.1 m/s and 14.9 m/s respectively. Thus, the finite length of the pad can have a significant effect on the predicted critical speed.[3] This effect has also been observed experimentally (Anderson and Knapp, 1989).

If we assume a realistic ratio of 3 between the radius of the frictional contact on the disk and the effective rolling radius of the tire, we find that these sliding speeds correspond to road speeds of 66 km/hr and 161 km/hr, respectively. It is instructive to compare these results with the prediction of critical speed based on the two half-plane model of sliding. In this model, the most unstable perturbation always corresponds to the largest permissible wavelength. Using the same assumptions as above, the two half-plane model predicts critical road speed of 1555 km/hr with friction material C and 34668 km/hr with material D indicating that the automotive disk brake system should be always stable under highway conditions. However, experimental investigations (Kreitlow et al., 1985; Abendroth, 1985; Anderson and Knapp, 1989) show that hot spots are developed at practical operating speeds. The finite disk thickness is clearly an important factor in this discrepancy.

5.2 The Effect of Friction Material Properties. The composition and composite structure of most friction materials offers scope for material "design." In other words, modifications might be made in the constituents or the manufacturing method to produce a material whose properties are in some sense optimal. Traditionally, this flexibility is used to achieve desirable frictional characteristics such as moderate fade behavior with increasing temperature. However, the possibility also exists to modify the thermal and/or elastic properties with a view to reducing the tendency for thermoelastic instability. We therefore consider the effect of these properties on the critical sliding speed.

We assume throughout this section that the disk is of cast iron, with properties as given in Table 1, and that the pad length is sufficiently long to support perturbations of the preferred wavelength, so that the critical speed will be defined by the minimum point in curves such as Fig. 2.

Elastic Modulus. If the friction material has a low elastic modulus, we might expect the applied contact load to be approximately uniformly distributed across the pad, discouraging the formation of hot spots. This argument, which is also supported by experimental observations (Anderson and Knapp, 1989), motivated the development of low modulus friction materials even before the connection between hot spots and thermoelastic deformation was discovered. Notice, however, that a compliant friction material will generally require a greater brake pedal movement to achieve a given braking torque. Typical friction materials have elastic moduli in the range $E = 0.5$ GPa to 10 GPa (Harding and Wintle, 1978).

The minimum dimensionless critical speed is shown in Fig. 5 as a function of the reciprocal of the elastic modulus. Results are shown for materials in which the remaining thermal and mechanical properties are those of materials C and D of Table 1. In each case, the critical speed is approximately linear with $1/E$, though the curves do not pass through the origin, instead converging on small but finite values as $1/E \to 0$ of 26 for material C and 35 for material D.

Coefficient of Thermal Expansion. Theoretical investigations of thermoelastic instability always show that the velocity of a sinusoidal perturbation is closer to that of the more conducting material than to that of the less good conductor. In automotive applications, the disk generally has a conductivity at least one order of magnitude higher than the pad and hence the disturbance moves slowly over the disk and rapidly over the pad. The effective Peclet number $c_1/k_1 m$ for the pad is therefore high, indicating that there will be relatively little thermal penetration of zero average thermal disturbances into the depth. It follows that the thermal distortion of the pad due to the perturbation will be small and hence that the expansion coefficient of the friction material should have little effect on the critical speed.

[3] A related restriction on permissible wavelengths is imposed on the disk by the requirement that an integral number of complete waves must be accommodated in the circumference. However, in the systems investigated here, the effects of this restriction are insignificant.

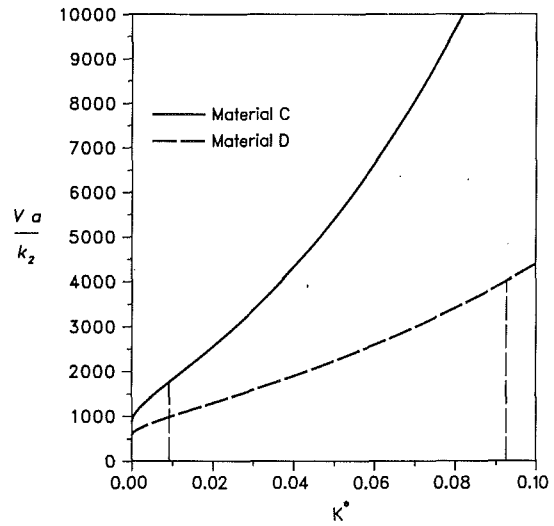

Fig. 6 The effect of thermal conductivity ratio, $K^* = K_1/K_2$, on the minimum critical speed

This conclusion is supported by the present results, which show that the minimum critical speed varies by less than 1 percent as the ratio of thermal expansion coefficients, α^*, is varied by a factor of 10 in either direction.[4]

Thermal Conductivity. Similar arguments lead us to expect that increasing the conductivity of the pad material will increase the critical sliding speed. This prediction is confirmed by the results shown in Fig. 6, where the minimum Va/k_2 is shown as a function of the conductivity ratio K^*, all other material properties being held constant. Experimental observations (Anderson and Knapp, 1989) also confirm this prediction, but we note that an undesirable practical consequence of increasing the pad conductivity is that more of the frictional heat will be directed into the pad. Convective cooling of the pad is less effective than that of the disk and the consequent rise in mean pad temperature may cause problems such as temperature-induced brake fade or vaporization of the brake fluid.

[4]Notice, however, that the argument depends on the disturbance having a velocity close to that of the disk. There is experimental evidence of hot spots stationary with respect to the pad in automotive systems, which might be associated with structural warping of the pad or with pressure perturbations varying in the radial rather than the circumferential direction. In this case, we should anticipate a significant dependence of critical speed on the thermal expansion coefficient of the pad material. This question is still under investigation.

7 Conclusions

Dow and Burton's analysis of frictionally excited thermoelastic instability has been extended to the case of a layer of finite thickness sliding between two half-planes, in order to evaluate the influence of finite disk thickness on the stability behavior of an automotive disk brake. The results show that with the layer geometry there is a preferred wavelength for instability, in contrast to the sliding of two half-spaces, where critical speed decreases monotonically with wavelength. The onset of instability is always characterized by an antisymmetric perturbation, corresponding to a "circumferentially buckled" deformation mode and leading to hot spots at alternating locations on the two sides of the disk. Using material properties and dimensions appropriate to current automotive practice, the layer model predicts critical speeds of the order of those observed in experiments, in contrast to the two half-space model that overestimates critical speeds by an order of magnitude.

References

Abendroth, H., 1985, "A New Approach to Brake Testing," SAE, 850080.

Anderson, A. E., and Knapp, R. A., 1989, "Hot Spotting in Automotive Friction Systems," *Intl. Conf. on Wear of Materials*, Vol. 2, pp. 673–680.

Barber, J. R., 1967, "The Influence of Thermal Expansion on the Friction and Wear Process," *Wear*, Vol. 10, pp. 155–159.

Barber, J. R., 1969, "Thermoelastic Instabilities in the Sliding of Conforming Solids," *Proc. Roy. Soc.*, Series A312, pp. 381–394.

Barber, J. R., 1992, *Elasticity*, Kluwer Academic Publishers, Dordrecht.

Burton, R. A., Nerlikar, V., and Kilaparti, S. R., 1973, "Thermoelastic Instability in a Seal-Like Configuration," *Wear*, Vol. 24, pp. 177–188.

Day, A. J., 1988, "An Analysis of Speed, Temperature, and Performance Characteristics of Automotive Drum Brakes," ASME JOURNAL OF TRIBOLOGY, Vol. 110, pp. 298–305.

Dow, T. A., and Burton, R. A., 1972, "Thermoelastic Instability of Sliding Contact in the Absence of Wear," *Wear*, Vol. 19, pp. 315–328.

Green, A. E., and Zerna, W., 1954, *Theoretical Elasticity*, Clarendon Press, Oxford.

Harding, P. R. J., and Wintle, J. B., 1978, "Flexural Effects in Disc Brake Pads," *Proc. Inst. Mech. Eng.*, Vol. 192.

Hewitt, G. G., and Musial, C., 1979, "The Search for Improved Wheel Materials," *Inst. Mech. Eng., Intl. Conf. on Railway Braking*, York, p. 101.

Kreitlow, W., Schrödter, F., and Matthäi, H., 1985, "Vibration and Hum of Disc Brakes under Load," SAE, 850079.

Lee, K., and Barber, J. R., 1993, "The Effect of Shear Traction on Frictionally-Excited Thermoelastic Instability," *Wear*, Vol. 160, pp. 237–242.

van Swaaij, J. L., 1979, "Thermal Damage to Railway Wheels," *Inst. Mech. Eng., Intl. Conf. on Railway Braking*, York, p. 95.

Thoms, E., 1988, "Disc Brakes for Heavy Vehicles," *Inst. Mech. Eng., Intl. Conf. on Disc Brakes for Commercial Vehicles*, C464/88, pp. 133–137.